Choked flow in water/CO_2 solutions on air-independent propulsion systems

Isidoro Martínez · Pedro A. Casas

Abstract We develop a simplified model of choked flow in pipes for CO_2-water solutions as an important step in the modelling of a whole hydraulic system with the intention of eliminating the carbon dioxide generated in air-independent submarine propulsion. The model is based on an approximate fitting of the homogeneous isentropic solution upstream of a valve (or any other area restriction), for given fluid conditions at the entrance. The relative maximum choking back-pressure is computed as a function of area restriction ratio. Although the procedure is generic for gas solutions, numeric values for the non-dimensional parameters in the analysis are developed only for choking in the case of carbon dioxide solutions up to the pure-water limit.

Keywords Choked flow · Flashing · Cavitation · Carbon dioxide water solutions · Two phase flow

1 Introduction

An air independent propulsion system (AIP) is any type of system that allows underwater navigation of a submarine boat with total independence from the Earth's atmosphere. Hydrocarbon-oxygen based AIP systems (with these two substances carried inside the submarine) are a particular case which produces great quantities of water and CO_2 during its operation.

Production of CO_2 in large quantities by a submerged submarine is an important problem because, at present, there is no easy way to store it on board, and its ejection outside the submarine needs to be carried out with low energy consumption and silently. A review of proposed exhaust gas management systems can be found in Potter et al. [1].

One of the options available for removing the CO_2 generated by a hydrocarbon-oxygen based AIP system is to dissolve it into seawater at low pressure inside the submarine, and then pump the solution outside. This option has three well-defined basic steps:

- Step 1: Introduction of sea water on board the submarine, lowering its pressure from operational depth to the value needed to carry out the CO_2 dissolution process.
- Step 2: Dissolution of CO_2 into seawater at constant (low) pressure, independently of the pressure value outside the submarine.
- Step 3: Discharge of the water/CO_2 solution outside the submarine, raising its pressure again to the value corresponding with operational depth.

One of the challenges presented by these steps 1–3 is to keep energy consumption as low as possible by using a work recovery system. Such systems make use of the power obtained in the reduction of pressure of the seawater flow entering the submarine, to increase the pressure of the CO_2 laden water flow leaving the submarine, and can be divided in two main categories:

- A. Two-stage energy recovery systems.
- B. Direct energy recovery systems.

I. Martínez (✉)
Universidad Politécnica de Madrid, 28040 Madrid, Spain
e-mail: isidoro.martinez@upm.es

P. A. Casas
Ministerio de Defensa, Madrid, Spain
e-mail: pcasalc@fn.mde.es

In group "A" systems, stages 1 and 3 are carried out by independent hydraulic machines (a motor and a pump, respectively), the shafts of which are fixed together in order to allow transmission of mechanical energy between both machines. Additionally, a small electric motor is attached to the common shaft in order to compensate for energy losses due to flow of water through on-board circuits.

In group "B" systems, stages 1 and 3 are carried out by a single hydraulic machine, which is composed of several cylinders connected alternately with the high and low pressure circuits, and thus cycled to allow the intake and discharge of water, with the process being controlled by suitable synchronization devices.

Systems "A" and "B" have one thing in common: both include elements (synchronization valves, connection ports, etc.) in which flashing and choked flow phenomena are significant when the working fluid is a water/CO_2 solution near saturation conditions.

Therefore, development of an analytical model able to predict choked flow phenomena is a fundamental step in the simulation process of hydrocarbon-oxygen based AIP systems, as in any other marine application related to flows of CO_2 laden water.

This paper is part of a broader work focused on the removal of carbon dioxide generated by the propulsion plant of submerged submarine navigation. Our goal here is to propose a simplified model for choked flow in pipe contractions, to be implemented in a digital simulator of the complete CO_2 removal system, enabling a comparative analysis of functional performances between different CO_2 removal solutions. The proposed model must be simple, easy to integrate into a larger program, and able to reduce computer execution time as much as possible.

The objective of the present paper is to present a formulation of the flow rate through a horizontal pipe with a contraction, for any possible geometry and pressure jump, but restricting the analysis to unsaturated entrance conditions (subcooled liquid). We base the analysis of choked flow on the simple homogeneous equilibrium model [2], i.e., on the assumption of thermodynamic equilibrium at every cross-section in the pipe (no slip between bubbles and the liquid matrix), and on the isentropic expansion process (i.e. adiabatic flow with no dissipation upstream of the restriction, an assumption not valid for capillary tubes); see also Yoon et al. [3] for more advanced models. As for the equation of state, we make use of the perfect fluid models of incompressible liquid for water and its solutions, and of ideal gas models for vapour and CO_2 bubbles.

The choking criterion adopted is the maximum flow rate when back pressure is lowered at constant geometry and entrance conditions. However, the isentropic model might still be valid for lower discharge pressures if an ideal converging–diverging nozzle were considered, instead of a valve or any other non-streamlined flow restriction. In reality, there are always some frictional losses, and the liquid may follow on through metastable states after saturation for a while without bubbling.

The problem then reduces to finding the mass flow rate as a function of downstream pressure, $\dot{m}(p_2)$, for a given pipe geometry (entrance area A_1 and exit area A_2), and liquid entrance conditions: pressure p_1, temperature T_1, and CO_2 mass fraction w_c.

A large body of literature exists on choked flow from a pressurized liquid reservoir, particularly concerning loss of coolant accidents (LOCA) in nuclear reactors, but the published material deals mostly with pure water, although some of studies include the effects of dissolved air or other low-solubility gases. Our problem of choked flow in a pipe is simpler than the related problem of a pressurized vessel discharge, where thermal disequilibrium and slip between the two phases modifies the model's maximum flow rate [4].

2 Formulation

For one-dimensional steady isentropic flow (i.e. non-dissipative adiabatic flow) through a horizontal variable-area duct, neglecting gravity, the laws of conservation of mass, entropy, and energy, can be expressed as follows:

$$\mathrm{d}(\rho u A) = 0 \tag{1}$$

$$\mathrm{d}s = 0 \tag{2}$$

$$\mathrm{d}h + u\mathrm{d}u = 0 \tag{3}$$

where u is the cross-section averaged speed, $\rho u A = \dot{m}$ is the mass flowrate, and h is the specific enthalpy. To integrate Eqs. (1)–(3) from entrance conditions 1 (subcooled liquid) to the end of isentropic flow conditions 2 (two-phase flow when choking), it is necessary to include the two-phase equilibrium relations (i.e. saturation conditions) plus the two-phase mean variable relationship with two-phase composition. Notice that with the homogeneous equilibrium model, the two-phase flow appears as soon as the saturation condition (solution-gas equilibrium) is reached, either before the contraction, at the throat, downstream behind it, or at no location.

The relations between mean fluid values and two phase fluid values, for specific volume ($v = 1/\rho$), entropy (s), and enthalpy (h), are of the form $v = w_l v_l + w_g v_g$ according to the definition of mass fractions, where v may stand for volume, entropy, or enthalpy, and w_l and w_g are the mass fraction of liquid and gas, respectively ($w_l = 1 - w_g$). These mean magnitudes take the form, after substituting for the perfect liquid and perfect gas models:

Table 1 Material properties used in the model [6]

Property	Value	Comments
ρ_l, liquid phase density	$\rho_l = 1000$ kg/m^3	Pure water at 15 °C, $\rho_l = 998$ kg/m^3 Seawater at 15 °C, $\rho_l = 1026$ kg/m^3
R, gas constant	$R_c = 189$ J/(kg K) for CO_2 $R_v = 462$ J/(kg K) for H_2O	
$c_{p,l}$, liquid thermal capacity	$c_{p,l} = 4180$ J/(kg K)	Seawater at 15 °C, $c_{p,l} = 3990$ J/(kg K)
$c_{p,g}$, gas thermal capacity	$c_{p,l} = 840$ J/(kg K) for CO_2 $c_{p,l} = 1900$ J/(kg K) for H_2O	
Δh, phase change enthalpy	Δh = 0.44 MJ/kg from solution to gas Δh = 2.4 MJ/kg from water to vapour	CO_2 solution enthalpy changed of sign H_2O vaporization enthalpy
S_c, CO_2 solubility in pure water	$S_c = 20 \times 10^{-6}$ (kg/m^3)/Pa at 15 °C	$S_c = 30 \times 10^{-6}$ (kg/m^3)/Pa at 5 °C $S_c = 14 \times 10^{-6}$ (kg/m^3)/Pa at 25 °C
$w_{c,sat}$, CO_2 saturation mass fraction	$w_{c,sat} = 2.0 \times 10^{-3}$ at 15 °C and 100 kPa (i.e. 2 g of CO_2 per kg of solution)	$w_{c,sat} = 3.0 \times 10^{-3}$ at 5 °C $w_{c,sat} = 1.4 \times 10^{-3}$ at 25 °C
p_{sat}, gas saturation	($p_{sat} = w_c \rho_l / S_c$)	(proportional to CO_2 content; see next row)
p_v, vapour pressure	$p_v = 1.7$ kPa at 15 °C (equivalent to $w_c = 0.034 \times 10^{-3}$)	$p_v = 0.87$ kPa at 5 °C (eq. $w_c = 0.026 \times 10^{-3}$) $p_v = 3.17$ kPa at 25 °C (eq. $w_c = 0.044 \times 10^{-3}$)

$$\frac{1}{\rho} = (1 - w_g)\frac{1}{\rho_l} + w_g \frac{RT}{p} \tag{4}$$

$$s - s_0 = (1 - w_g)\left(c_{p,l} \ln \frac{T}{T_0}\right) + w_g \left(\frac{\Delta h}{T} + c_{p,g} \ln \frac{T}{T_0} - R \ln \frac{p}{p_0}\right) \tag{5}$$

$$h - h_0 = (1 - w_g)\left[c_{p,l}(T - T_0) + \frac{p - p_0}{\rho_l}\right] + w_g\left[\Delta h + c_{p,g}(T - T_0)\right] \tag{6}$$

where s_0 and h_0 are the reference entropy and enthalpy values at T_0 and p_0, and all material parameters are assumed to have constant values (see Table 1).

Differentiating these expressions (neglecting the variation of the gasification and vaporization enthalpies with temperature, and assuming small variations in T and p):

$$\mathrm{d}\frac{1}{\rho} = -\frac{1}{\rho_l}\mathrm{d}w_g + w_g \mathrm{d}\frac{RT}{p} + \frac{RT}{p}\mathrm{d}w_g \tag{7}$$

$$\mathrm{d}s = (1 - w_g)\frac{c_{p,l}}{T}\mathrm{d}T + w_g\left(-\frac{\Delta h}{T^2}\mathrm{d}T + \frac{c_{p,g}}{T}\mathrm{d}T - \frac{R}{p}\mathrm{d}p\right) + \frac{\Delta h}{T}\mathrm{d}w_g \tag{8}$$

$$\mathrm{d}h = (1 - w_g)\left(c_{p,l}\mathrm{d}T + \frac{1}{\rho_l}\mathrm{d}p\right) + w_g c_{p,g}\mathrm{d}T + \Delta h \mathrm{d}w_g \tag{9}$$

As for the two-phase equilibrium conditions, we consider two separate cases:

- For pure water, the liquid–vapour equilibrium pressure–temperature relationship, given by the Clausius–Clapeyron equation:

$$\left.\frac{\mathrm{d}p}{\mathrm{d}T}\right|_{sat} = \frac{\Delta h}{T\Delta v} \simeq \frac{\Delta h}{\frac{RT^2}{p}} \quad \rightarrow p_v(T) = p_{v_0} \exp\left[\frac{-\Delta h}{R}\left(\frac{1}{T} - \frac{1}{T_0}\right)\right] \tag{10}$$

  where $p_v(T)$ is the vapour pressure of pure water at temperature T, and (T_0, p_{v_0}) a point in the vapour–pressure curve (e.g. $T_0 = 373$ K and $p_0 = 100$ kPa); e.g., at $T_1 = 288$ K (15 °C), $p_v = 1.7$ kPa (Table 1).

- For water/CO_2 solutions, the liquid–gas equilibrium pressure-concentration relationship, which can be linearly approximated according to Henry's law in the form:

$$p_{sat}(w_c) = \frac{\rho_l}{S_c} w_c \tag{11}$$

  where ρ_l is the solution density, w_c the CO_2 mass fraction in solution, and S_c is the solubility (values for pure water in Table 1; solubility in seawater is slightly less). Equation (11) serves also to find the saturating mass fraction for a given pressure and temperature; e.g., for pure water at 288 K [$S_c = 20 \times 10^{-6}$ (kg/m^3)/Pa], and $p = 100$ kPa, the saturating CO_2 mass fraction is $w_{c,sat} = pS_c/\rho_l = 0.002$ (2 g/kg), so that, if entrance CO_2 mass is $w_c = 0.1$ g/kg, pressure would have to drop to $p_{sat} = w_c \rho_l / S_c = 0.1 \times 10^{-3} \times 1000/(20 \times 10^{-6}) = 5$ kPa to attain liquid–gas equilibrium.

Under the conditions envisaged in this work (rather cold sea water), even a small amount of dissolved CO_2 (5 % relative to saturation in the example above) already means that CO_2 gas bubbling starts sooner than H_2O vapour bubbling (at 1.7 kPa), and that we may neglect H_2O concentration in the gas phase. The CO_2 mass fraction, below which vapour bubbling overcomes gas bubbling, is obtained from $w_{c,sat}(T, p_v) = p_v\,(T)S_c/\rho_l$, which has been used to compute the 'equivalent' mass fractions presented

in Table 1. In our analysis we consider only pure CO_2 bubbles ($p_{sat}(w_c) \gg p_v(T)$) or pure H_2O bubbles ($p_{sat}(w_c) \ll p_v(T)$), without paying attention to two-component bubbles ($p_{sat}(w_c) \sim p_v(T)$).

Notice that the mass balance for H_2O in the case of two phase flow with pure CO_2 bubbles is $\dot{m}(1-w_c) = \dot{m}_l(1-w_{c,sat})$, where $\dot{m}$ is the entry flow rate, and $\dot{m}_l$ is the exit flow rate in liquid phase, saturated with CO_2, because equilibrium is assumed. With $\dot{m} = \dot{m}_l + \dot{m}_g = \dot{m}(1-w_g) + \dot{m}w_g$ the mass balance for H_2O becomes:

$$1 - w_c = (1 - w_g)(1 - w_{c,sat}). \tag{12}$$

The problem is to be solved for both small values of total CO_2 mass fraction ($w_c \ll 1$) and small values of gas mass fraction (notice that the CO_2 mass balance implies $w_g \leq w_c$). With this assumption, and neglecting the liquid specific volume, $1/\rho_l$, against the gas specific volume, RT/p, Eqs. (7)–(9) simplify to:

$$\mathrm{d}\frac{1}{\rho} = \frac{RT}{p}\mathrm{d}w_g \tag{13}$$

$$\mathrm{d}s = \frac{c_{p,l}}{T}\mathrm{d}T + \frac{\Delta h}{T}\mathrm{d}w_g \tag{14}$$

$$\mathrm{d}h = c_{p,l}\mathrm{d}T + \frac{1}{\rho_l}\mathrm{d}p + \Delta h\,\mathrm{d}w_g, \tag{15}$$

with which the entropy and energy, Eqs. (2) and (3), become (the latter combined with the former):

$$c_{p,l}\mathrm{d}T + \Delta h\,\mathrm{d}w_g = 0 \tag{16}$$

$$\frac{1}{\rho_l}\mathrm{d}p + u\mathrm{d}u = 0. \tag{17}$$

Notice that the isentropic condition (16) implies that the process is nearly isothermal, due to the smallness of the gas mass fractions considered (for $\Delta w_g = 10^{-3}$, since $\Delta T = -(\Delta h/c_{p,l})\Delta w_g = (0.44 \times 10^6/4180) \times 10^{-3} = 0.1$ K).

Equation (17) can be easily integrated from conditions 1–2:

$$\frac{1}{\rho_l}(p_2 - p_1) + \frac{u_2^2 - u_1^2}{2} = 0, \tag{18}$$

which is similar to the traditional Bernoulli equation, $p_1 + \rho_l u_1^2/2 = p_2 + \rho_l u_2^2/2$, but now applicable to two-phase flows. Notice the difference between the density of the liquid phase, ρ_l, which we have assumed to be of constant value and equal to the subcooled liquid at entrance conditions, $\rho_l = \rho_1$, and the density at the end section considered, ρ_2, which will be taken as equal to the liquid density only if there is no two-phase transition; otherwise, saturation will be assumed and (4) applied.

Eliminating velocities in (18) with $\dot{m} = \rho_1 u_1 A_1 = \rho_2 u_2 A_2$, allows finding the mass flow rate wanted:

$$\dot{m} = \sqrt{\frac{2(p_2 - p_1)}{\rho_l\left(\frac{1}{A_2^2\rho_2^2} - \frac{1}{A_1^2\rho_1^2}\right)}}, \tag{19}$$

although we prefer to quantify the flow in terms of the dynamic pressure at the entrance, q_1 (keep in mind that $\dot{m}_1 = \dot{m}_2$ but $q_1 \neq q_2$):

$$q_1 \equiv \frac{1}{2}\rho_1 u_1^2 = \frac{\dot{m}^2}{2\rho_1 A_1^2} = \frac{p_1 - p_2}{\left(\frac{A_1\rho_1}{A_2\rho_2}\right)^2 - 1}. \tag{20}$$

Density at the entrance is $\rho_1 = \rho_l$ (subcooled liquid always assumed), but density at the end of the isentropic expansion can be either $\rho_2 = \rho_l$ if the liquid does not reach saturation (i.e. if $p_2 \geq p_{sat}$), or, if two-phase flow develops (CO_2/water saturation), substitution of the H_2O balance (12) in (4) and with the isothermal approximation justified by the isentropic flow, yields:

$$\frac{1}{\rho_2} = \frac{1}{\rho_l}\left[1 + K_c\left(\frac{p_{sat,1}}{p_2} - 1\right)\right], \tag{21}$$

where $K_c \equiv S_c R_c T_1$ (from Table 1, at 288 K and 100 kPa, $K_c = 1.1$). Notice that $p_{sat,1} = w_c\rho_l/S_c$ is the saturation pressure for entry conditions (which is why we use the subindex '1'), although it applies everywhere in view of the isothermal approximation, and that Eq. (21) is valid in the range $p_v(T_1) \ll p_2 \leq p_{sat,1}$, i.e. for $w_c \gg p_v(T)S_c/\rho_l$.

We may use (21) to find the speed of sound, c, in the two-phase fluid, which takes a simple form in this case where K_c is close to 1:

$$\frac{1}{\rho} = \frac{1}{\rho_l}\left[1 + K_c\left(\frac{p_{sat,1}}{p} - 1\right)\right] = \frac{1}{\rho_l}\left[1 + K_c\frac{p_{sat,1}}{p} - K_c\right]$$
$$\approx \frac{K_c p_{sat,1}}{\rho_l p} \rightarrow p = \frac{K_c p_{sat,1}}{\rho_l}\rho = w_c R_c T_1 \rho$$
$$\Rightarrow \quad c \equiv \sqrt{\left.\frac{\partial p}{\partial \rho}\right|_s} \approx \sqrt{w_c R_c T_1} \tag{22}$$

i.e. the speed of sound is roughly independent of the gas mass fraction, depending just on the total CO_2 content, with a maximum value of:

$$c_{max} \approx \sqrt{w_{c,sat} R_c T_1} = \sqrt{\frac{p_1 S_c}{\rho_l} R_c T_1} \tag{23}$$

e.g. in our case of $p_1 = 100$ kPa and $T_1 = 288$ K ($w_{c,sat} = 2$ g/kg), $c_{max} = 10$ m/s, much lower than the speed of sound in liquid water (1500 m/s) or in CO_2 gas (260 m/s) at those conditions. Mind that $w_{c,sat}$ in (23) stands for the maximum value that w_c can reach at the pipe

entrance, whereas in (12) it is the CO_2 mass fraction in the liquid phase in two-phase equilibrium at the exit.

For very low CO_2 contents, $w_c \ll p_v(T)S_c/\rho_l$ (e.g. $w_c \ll 34 \times 10^{-6}$ for 288 K and 100 kPa, Table 1), choking bubbles can be considered as being made of pure vapour. Substitution of the isentropic balance (16) in (13) with the saturation model (10), and integrating, yields a solution similar to (21):

$$\frac{1}{\rho_2} = \frac{1}{\rho_l}\left[1 + K_v\left(\frac{p_{sat,1}}{p_2} - 1\right)\right] \tag{24}$$

where $K_v \equiv \rho_l c_{p,l} R_v^2 T^3/((\Delta h)^2 p_{v,1})$ (from Table 1, at 288 K and 100 kPa, $K_v = 2200$). It is worth computing the derivative of fluid density with pressure just at the onset of two phase flow, which can be obtained from (21) to be $d\rho_2/dp_2|_{sat} = (\rho_l/p_{sat,1})K_c$, and from (24) to be $d\rho_2/dp_2|_{sat} = (\rho_l/p_{sat,1})K_v$, showing that the slope can be mild when CO_2 saturation occurs first ($K_c = 1.1$) but is huge ($K_v = 2200$ and augmented by a lower $p_{sat,1}$) when water-vapour saturation occurs first; i.e. in our case of seawater, saturation by carbon dioxide may yield a smooth choking (a smooth flow rate saturation), but, without dissolved gases, vapour saturation occurs in an abrupt manner (with a kink in the flow rate dependence with back pressure).

A procedure similar to (22) can be used to estimate the speed of sound in the case of pure-vapour bubbles (but now with $K_v = 2200 \gg 1$), with the final result:

$$c = \frac{p_v(T_1)\Delta h}{\rho R_v T_1 \sqrt{c_{p,l} T_1}}, \tag{25}$$

where ρ is the two-phase density. In our case of $T_1 = 288$ K ($p_v = 1.7$ kPa), for $\rho = 1000$ kg/m^3, we get $c_{max} = 0.03$ m/s, much lower than the speed of sound in liquid water (1500 m/s) or in pure vapour at 15 °C (420 m/s). The smallness of the speed of sound in liquid–vapour equilibrium (LVE) can be understood directly from the definition of c in (22), because we showed that the isentropic process can be approximated by an isothermal process, which is equivalent to an isobaric process in LVE, and thus to a vanishing sound speed. Such small sound speeds are really the cause of the flow becoming choked, since pressure changes (travelling at sonic speed) cannot move upstream.

Comparing results obtained with Eq. (25) with data from García Cascales [5] for pure water at 373 K, differences are within 5 % for two-phase densities from 1000 kg/m^3 down to 20 kg/m^3 (i.e. from incipient bubbling, $w_g = 0$, to relatively large vapour mass fractions, $w_g < 0.03$).

The analysis is now completed; we have obtained explicit expressions that give the mass flow rate $\dot{m}$ in (19) or the dynamic pressure in (20) as a function of geometry, material properties, and entrance and exit conditions. The general functional dependence, in non-dimensional parameters, is of the form:

$$\frac{q_1}{p_1} = f\left(K_c, K_v, \frac{p_{v,1}}{p_{sat,1}}, \frac{p_{sat,1}}{p_1}, \frac{A_2}{A_1}, \frac{p_2}{p_1}\right). \tag{26}$$

The first two parameters in (26) may be assumed constant in the present work, with values $K_c = S_c R_c T_1 = 20 \times 10^{-6} \times 189 \times 288 = 1.1$ and $K_c = \rho_l c_{p,l} R_v^2 T^3/(.) = 1000 \times 4180 \times 462^2 \times 288^3/((2.4 \times 10^6)^2 \times 1700) = 2200$. The third parameter, $p_{v,1}/p_{sat,1}$, marks the validity of the pure-CO_2 bubbles assumption ($p_{v,1}/p_{sat,1} \ll 1$) or pure-H_2O bubbles assumption ($p_{v,1}/p_{sat,1} \gg 1$). The flow dependence with the remaining three parameters is worked out below to produce the desired results.

3 Results

The main result in this work can be summarised in the general relation between densities (exit/entry) from (21) and (24), namely:

$$\frac{\rho_2}{\rho_l} = \frac{1}{1 + K\left(\frac{p_{sat,1}}{p_2} - 1\right)} \quad \text{with} \quad \begin{cases} K = K_c & \text{if } p_v(T_1) < p_2 < p_{sat,1}(w_c) \\ K = 0 & \text{if } p_2 > p_{sat,1}(w_c) \end{cases} \tag{27}$$

and consequently:

$$\frac{u_2}{u_1} = \frac{\rho_1}{\rho_2}\frac{A_1}{A_2}, \quad \frac{q_1}{p_1} = \frac{1 - \frac{p_2}{p_1}}{\left(\frac{\rho_1}{\rho_2}\right)^2\left(\frac{A_1}{A_2}\right)^2 - 1}. \tag{28}$$

Figure 1 presents some results of the steady flow in a pipe corresponding to a typical CO_2 laden case with $p_{sat,1}/p_1 = 0.8$, and $A_2/A_1 = 0.5$, with the criterion that choking occurs when the flow no longer increases when p_2 is decreased, while p_1 is maintained constant.

The result is as expected: for constant entry pressure, if we start from evacuated discharge conditions ($p_2 = 0$), the flow stays choked, that is, mass flow rate invariant with back pressure (with scaled dynamic pressure $q_1/p_1|_{choked} = 0.070$ in Fig. 1), until the critical condition, $p_2/p_1 = 0.73$, and then, after a small accommodation range, a linear dependence of dynamic pressure with pressure jump, $q_1 = C'\Delta p$, corresponding to a square root dependence of the mass flow rate predicted by Bernoulli's equation, $\dot{m} = C\sqrt{\Delta p}$.

The dashed line in Fig. 1 corresponds to the supersonic flow solutions that might develop in an isentropic converging–diverging nozzle with a throat in between stages 1 and 2 corresponding to areas and pressures A_2/A_1 and p_2/p_1 at the ends. To better appreciate this all-isentropic solution,

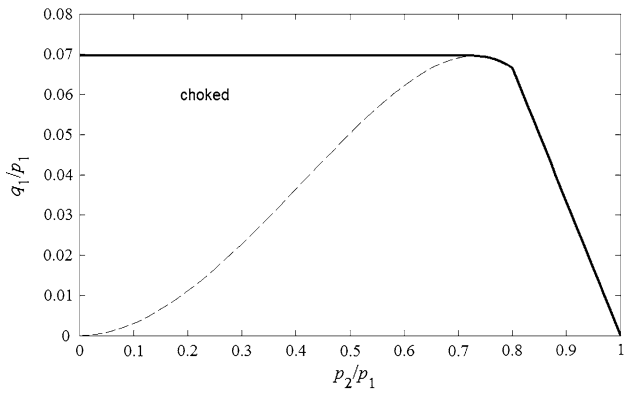

Fig. 1 Entry flow dynamic pressure, q_1, versus imposed back pressure, p_2, both made non-dimensional with entry pressure, p_1, for a typical case of a laden CO_2/water solution with $p_{sat,1}/p_1 = w_c\rho_l/(S_c p_1) = 0.8$, and a contraction $A_2/A_1 = 0.5$

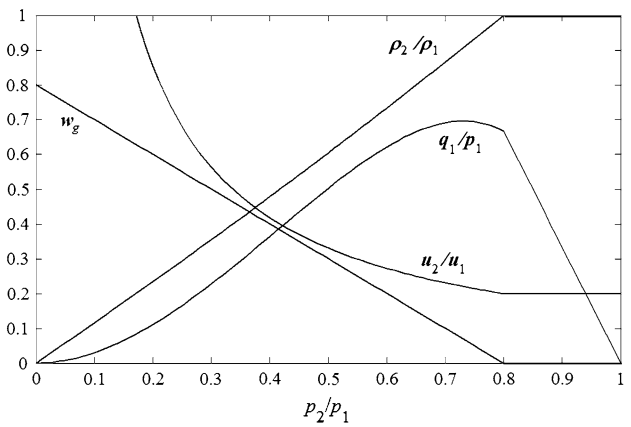

Fig. 2 Combined plot of relative dynamic pressure, $q_1/p_1 \times 10$, relative exit speed, $(u_2/u_1)/10$, relative exit density, ρ_2/ρ_1, and exit gas mass fraction, $w_g \times 500$, versus relative back pressure p_2/p_1, for a typical case of a CO_2/water solution with, $A_2/A_1 = 0.5$ and the following entrance conditions: $p_1 = 100$ kPa, $T_1 = 288$ K, $\rho_l = 1000$ kg/m^3, $w_c = 1.6$ g/kg (so that $p_{sat,1}/p_1 = \rho_l w_c/(S_c p_1) = 0.8$), and $A_2/A_1 = 0.5$

the evolution of relative dynamic pressure, q_1/p_1, relative exit speed, u_2/u_1, relative exit density, ρ_2/ρ_1, and exit gas mass fraction, w_g, are presented in Fig. 2, scaled appropriately to fit in a combined plot, for the same example as in Fig. 1 (compare the q_1/p_1 curves in both plots). One can see how exit-speed monotonically grows when back pressure decreases from $p_2/p_1 = 1$ (in spite of the maximum being achieved on mass flow rate), how exit-density monotonically diminishes, and how the mass fraction of the CO_2 gas released grows from zero to the value of the mass fraction of CO_2 initially dissolved in the unsaturated liquid at the entrance. Contrary to the choking in a converging–diverging gas flow nozzle, flow speed is not equal to sound speed in the necking (i.e., Mach number never equals unity), changing abruptly from subsonic to supersonic,

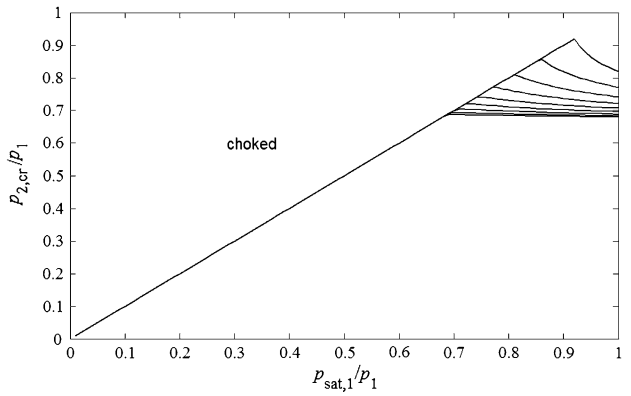

Fig. 3 Critical downstream pressure, $p_{2,cr}/p_1$, as a function of entry CO_2 mass fraction, w_c ($p_{sat,1}/p_1 = w_c\rho_l/(S_c p_1)$), for several area ratios $A_2/A_1 = 0.1$, 0.2, 0.3, 0.4, 0.5, 0.6, 0.7, 0.8, and 0.9, not labelled (they coincide for most of the range, $A_2/A_1 = 0.9$ being the upper one)

because of the discontinuity in sound speed at liquid saturation (from 1500 m/s to less than 10 m/s in our case), in spite of the continuity in flow speed and fluid properties at the transition.

The reason isentropic mass flow rate decreases after the maximum (when back pressure decreases from $p_2/p_1 = 1$), can only be explained by an intermediate necking in the variable-area duct from 1 to 2, required to adjust back pressure at 2 for given end areas, A_2/A_1, In practical non-streamlined pipe contractions, as in a valve, downstream flow separates from the walls, creating eddies where part of the mechanical energy of the flow passes to thermal energy, with a consequent entropy generation, and the isentropic analysis is valid only from the entrance to the neck, where the flow flashes, locally attaining the speed of sound, and preventing any further downstream pressure decrease to be transmitted upstream.

Our main interest is on finding the choking conditions, i.e., on finding the maximum in the q_1-p_2 curves such as the one presented in Fig. 1. If we just keep the critical pressure obtained in that way (i.e. the abscissa of the maximum, $p_{2,cr}/p_1 = 0.73$ in Fig. 1 for $p_{sat,1}/p_1 = 0.8$ and $A_2/A_1 = 0.5$), and represent it as a function of $p_{sat,1}/p_1$, we get the overall picture of choking conditions shown in Fig. 3, as a function of entry condition, $p_{sat,1}/p_1 = w_c\rho_l/(S_c p_1)$, and contraction A_2/A_1.

We see in Fig. 3 that the condition for choked flow is $p_2 = p_{sat,1}$ for small and medium values of $p_{sat,1}/p_1$, i.e. for CO_2 mass fractions in water w_c not close to the saturation ($w_c < w_{c,sat} = p_1 S_c/\rho_l$). But, for nearly saturated solutions, choking takes place at lower discharge pressures, $p_{2,choked} < p_{sat,1}$, as can be seen in Fig. 3 (and more clearly in Fig. 1, where it is apparent that the maximum flow rate is larger than that corresponding to $p_{2,cr} = p_{sat,1}$). The reason the flow rate keeps increasing after saturation is reached and a two-phase flow develops is that the increase

in speed caused by lowering exit pressure (Fig. 2), more than compensates for the decrease in density associated with the formation of CO_2 bubbles. However, further flashing changes this balance and the decrease in two-phase density predominates.

Finally, note that we have presented results only for the choking by CO_2 bubble formation, disregarding the formation of water vapour, which, as deduced in the former analysis, would take over in importance for very small CO_2 mass fractions, $p_{sat,1} \ll p_v(T_1)$.

4 Conclusions

The aim of this paper was to obtain a simple analytical model that predicts choking conditions in the flow of CO_2/water solutions through contractions in a horizontal pipe, for given subcooled entry conditions (to be integrated into a global model of the CO_2 removal system for air-independent submarine propulsion).

We conclude from the present analysis that a good enough model for this purpose may be to approximate the curves resembling a flag in Fig. 3, by horizontal straight lines with the following fitting: the maximum choking back pressure, $p_{2,cr,max}/p_1$, for a given area ratio, A_2/A_1, is:

$$\frac{p_{2,cr,max}}{p_1} = 0.7 + 0.3\left(\frac{A_2}{A_1}\right)^4 \tag{29}$$

such that the choking takes place for $p_{2,cr,max}/p_1$ given by:

$$\left.\begin{array}{ll} \text{For } \dfrac{p_{sat,1}}{p_1} \geq 0.7 + 0.3\left(\dfrac{A_2}{A_1}\right)^4 & \dfrac{p_{2,cr}}{p_1} = 0.7 + 0.3\left(\dfrac{A_2}{A_1}\right)^4 \\ \text{For } \dfrac{p_{sat,1}}{p_1} < 0.7 + 0.3\left(\dfrac{A_2}{A_1}\right)^4 & \dfrac{p_{2,cr}}{p_1} = \dfrac{p_{sat,1}}{p_1} \end{array}\right\} \tag{30}$$

which is plotted in Fig. 4 to compare with Fig. 3; the maximum deviation is 9 %, with typical deviations less than 5 %.

Notice again that we have presented results only for choking by CO_2 bubble formation ($p_{sat,1} \gg p_v(T_1)$), disregarding the formation of water vapour, which, as deduced in the former analysis, would take over in importance for very small CO_2 mass fractions, $p_{sat,1} \ll p_v(T_1)$. The intermediate region ($p_{sat,1} \sim p_v(T_1)$), and the CO_2-weak region down to the pure water limit, $p_{sat,1} \ll p_v(T_1)$, would demand a more detailed analysis, accounting for both components (CO_2 and H_2O) in the gas phase.

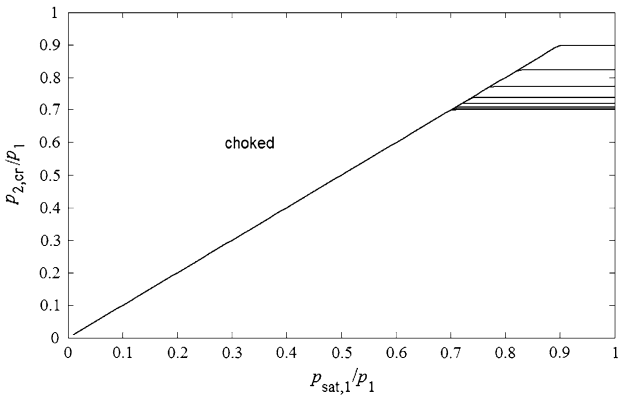

Fig. 4 Approximation of critical downstream pressure, $p_{2,cr}$, dependence with entry CO_2 mass fraction, w_c ($p_{sat,1}/p_1 = w_c\rho_l/(S_c p_1)$)

We have also developed expressions for the speed of sound in the two phase fluid, both in the case of CO_2 bubbles in equilibrium with its solution, and in the case of pure vapour with liquid water, with perfect correlations with other data available for the latter.

We have not found in the literature experimental values to compare with the choking limits developed here.

References

1. Potter IJ, Clavelle E, Reader GT, Kady J, Carl M (2000) Exhaust gas management systems for underwater heat engines. In: Proceedings of the 2000 international symposium on underwater technology, pp 273–278. doi:10.1109/UT.2000.852556
2. Brennen CE (2005) Fundamentals of multiphase flow. Cambridge University Press, Cambridge
3. Yoon HJ, Ishii M, Revankar ST (2006) Choking flow modeling with mechanical non-equilibrium for two-phase two-component flow. Nucl Eng Des 236:1886–1901
4. Valero E, Parra IE (2002) The role of thermal disequilibrium in critical two-phase flow. Int J Multiph Flow 28:21–50
5. García Cascales JR (2009) Conservative numerical schemes for unsteady 1D two phase flow. Doctoral Thesis, Universidad Politécnica de Cartagena, Spain
6. Carroll JJ, Slupsky JD, Mather AE (1991) The solubility of carbon dioxide in water at low pressure. J Phys Chem Ref Data 20(6): 1201–1209